Decomposing Effective Radiative Forcing due to Aerosol Cloud Interactions by Global Cloud Regimes

Tom Langton[1], Philip Stier[1], Duncan Watson-Parris[1], Jane P. Mulcahy[2]

[1]Atmospheric, Oceanic and Planetary Physics, Department of Physics, University of Oxford, Oxford, UK
[2]Met Office, Exeter, UK

Key Points:

- The majority of effective radiative forcing in HadGEM3-GA7.1 comes from stratocumulus clouds
- Forcing from marine stratocumulus clouds is highly sensitive to aerosol perturbations

Corresponding author: Tom Langton, thomas.langton@physics.ox.ac.uk

Abstract

Quantifying Effective Radiative Forcing due to aerosol-cloud interactions (ERF_{ACI}) remains a largely uncertain process, and the magnitude remains unconstrained in general circulation models. Previous studies focus on the magnitude of ERF_{ACI} arising from all cloud types, or examine it in the framework of dynamical regimes. Aerosol forcing due to aerosol-cloud interactions in the HadGEM3-GA7.1 global climate model is decomposed into several global observational cloud regimes. Regimes are allocated to model gridboxes and forcing due to aerosol-cloud interactions is calculated on a regime-by-regime basis with a 20–year meaning period. Patterns of regime occurrence are in good agreement with satellite observations. ERF_{ACI} is then further decomposed into three terms, representing radiative changes within a given regime, transitions between different cloud regimes, and nonlinear effects. The total global mean ERF_{ACI} is -1.8 Wm^{-2}. When decomposed, simulated ERF_{ACI} is greatest in the stratocumulus regime (-0.75 Wm^{-2}).

Plain Language Summary

The effect of anthropogenic aerosol emissions on clouds is highly uncertain in climate models. Many previous attempts to reduce this uncertainty have focused on examining all cloud types as a whole. This work sets out a framework to examine one measure of aerosol-cloud interactions when the effect is split by different cloud types. This framework is applied to the HadGEM3-GA7.1 climate model. It is hoped that this will lead to a greater understanding of how these interactions manifest themselves in different cloud types, and that this methodology will promote the use of constraints on specific cloud types, to provide potentially greater reductions in the aforementioned uncertainty.

1 Introduction

The radiative forcing (RF) produced by aerosol remains a large source of uncertainty in climate models (IPCC, 2013). General Circulation Models (GCMs) show a wide range in their predictions of aerosol forcing, through the uncertainty in effective radiative forcing, due to aerosol-cloud interactions (ERF_{ACI})(Bellouin et al., 2020).

Aerosol-cloud interactions are driven by a number of different effects, occurring on different timescales. Instantaneous effects will drive changes in the instantaneous radiative forcing due to aerosol-cloud interactions (RF_{ACI}). For instance the Twomey effect, which predicts that a cloud with constant liquid water content will increase in optical depth when aerosol loading increases (Twomey, 1977). Effects that occur over longer timescales will instead affect the ERF_{ACI}, for instance the 2^{nd} indirect effect (Albrecht, 1989) predicts that aerosol leads to increased liquid water path and cloud lifetime (Rotstayn, 1999). These effects are difficult to constrain however, due to the need for parameterisation in GCMs owing to the microscopic nature of aerosol-cloud interactions, the huge heterogeneity in aerosol loading, and the uncertainty in the exact nature of these mechanisms themselves (Boucher et al., 2013).

Even within GCMs, the indirect forcing by aerosol can vary wildly. As can be seen in Mulcahy et al. (2018), the change in forcing due to aerosol-cloud interactions (ERF_{ACI}) between the GA7.0 and GA7.1 (Global Atmosphere) science configurations of HadGEM3 (Hadley Centre Global Environmental Model version 3) was 1.04 Wm^{-2}. As a result, it remains a question as to exactly why these changes can bring about such large variation in ERF_{ACI}, and which types of cloud are the most sensitive to these changes in the model. One way to do this is to examine the ERF_{ACI} when it is decomposed into cloud regimes. This will also give a detailed insight into the way cloud processes are modelled, and provides a pathway to incorporate results from observations and high resolution modelling, as these will make predictions relating to specific cloud regimes.

Regime-based analysis of clouds uses joint histograms of cloud top pressure (CTP) and cloud optical depth (COD), and was pioneered by Jakob and Tselioudis (2003), using the data produced by International Satellite Cloud Climatology Project (ISCCP; (Rossow & Schiffer, 1999)). This analysis has had success when applied to observations. For instance, several studies have determined the sensitivity of different cloud properties to AOD in a regime-based framework (Gryspeerdt & Stier, 2012; Oreopoulos et al., 2020). In addition, Schuddeboom et al. (2018) examined differences in the cloud radiative effect (CRE) between models and observations. What has not been done however, is to examine on a regime-by-regime basis the indirect radiative forcing by aerosol. It reasonable to believe, in light of these papers, that different cloud regimes may react differently to an increase in aerosol emissions, and hence have varying total contributions to the aerosol forcing. When decomposed into regimes, it will also be possible to examine the modelled sensitivities of each regime, for instance the sensitivity of cloud albedo to aerosol loading.

This paper sets out a framework to analyse indirect aerosol forcing by cloud regime, and applies this methodology to analyse the forcing from HadGEM3. This methodology can provide useful insight into how different models calculate aerosol processes. In addition, the forcing can be quantified in terms of changes in the average properties of each regime, and also to account for differing relative frequency of occurence (RFO) of regimes between present-day and pre-industrial time periods.

2 Methodology

2.1 Model and Experimental Design

This study makes use of 2 different model runs of HadGEM3 GA7.1 global model and the Global Land configuration version 7.1 (GL7.1) (Walters et al., 2019). A 20-year run is performed for both a present-day (1988–2008) and pre-industrial (1850 emissions) time period, both at N96 resolution ($1.875^\circ \times 1.25^\circ$) with 85 vertical levels. The aerosol-cloud interactions are handled by the Unified Model Physics scheme, described in Mulcahy et al. (2018). Cloud droplet number concentrations are diagnosed by the UK Chemistry and Aerosol model, using the Global Model of Aerosol Processes (GLOMAP-mode) (Mann et al., 2010) coupled to the single moment PC2 cloud microphysics (Wilson et al., 2008) via the Abdul-Razzak Ghan activation scheme (Abdul-Razzak & Ghan, 2000) as described in West et al. (2014). The emissions used are the present day Coupled Model Intercomparison Project Phase 6 (CMIP6) emissions datasets (Hoesly et al., 2018). For the 1850 emissions, anthropogenic aerosol emissions were reverted to their pre-industrial estimates, while natural emissions, sea ice coverage, and sea surface temperatures were kept identical to the present day run.

The CFMIP Observational Simulator Package (COSP; Bodas-Salcedo et al. (2011)) is used to generate the joint histograms of CTP and COD (τ) available from the Moderate Resolution Imaging Spectroradiometer (MODIS) D3 products. As COSP is designed to mimic the output of MODIS, these histograms are only available on sunlit points.

Data is generated every radiation timestep (1 hour), and regimes can be allocated on daylit points only. As COSP only produces data on daylit points, the nighttime LW forcing is calculated for all cloud types, and then divided amongst the regimes proportionally to their daytime RFO.

The PC2 cloud microphysics scheme does not include convective microphysics, however there are interactions between convective clouds and the large-scale microphysics, as detrained water is passed to the large-scale scheme. This means that while aerosols in the region of deep convective regimes will not accurately interact with the clouds as they would in an LES model, they will produce a signal, although this signal could be difficult to interpret accurately.

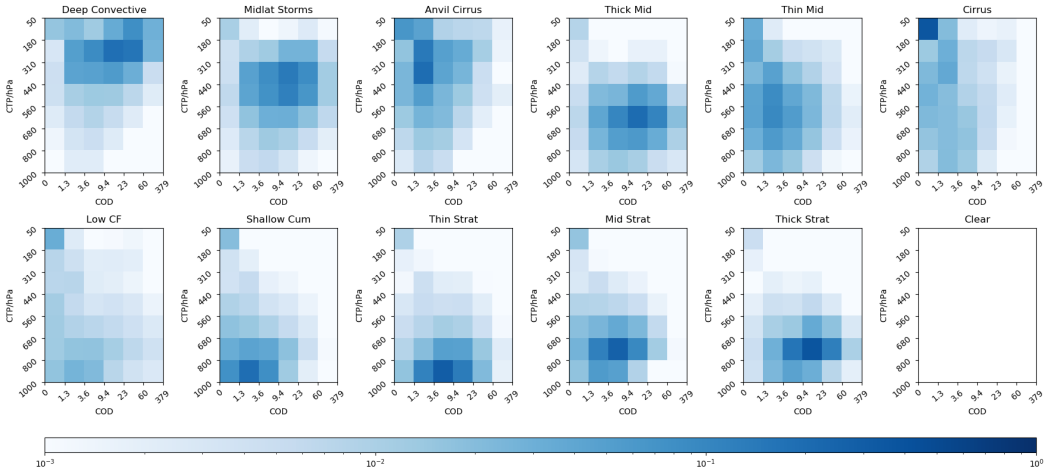

Figure 1. Histograms showing the 12 cluster centroids used in this analysis, as taken from Tselioudis et al. (2013). Shading represents cloud fraction. The clear regime was assigned by clustering on the other 11 regimes, and then applying a CF dependent mask to the gridboxes. The three different stratocumulus regimes were all merged into one cluster post-allocation.

2.2 Regime Allocation

Cloud regime definitions were taken from the work of Tselioudis et al. (2013), which defined a set of 11 Global Weather States (GWS) from ISCCP observations using a k-means clustering algorithm (Anderberg, 2014), which clusters on gridbox mean cloud top pressure (CTP), cloud optical depth (COD), and total cloud fraction (CF). These are depicted visually in figure 1.

These cloud regimes can be seen to somewhat mimic classical cloud types. Gridboxes with CF $\leqslant$ 0.5% are allocated to a separate clear-sky regime. In this analysis, the three stratocumulus regimes defined by Tselioudis et al. (2013) are merged into a single regime after the standard k-means allocation has occurred, in order to provide a more realistic estimate of stratocumulus forcing, by removing the transition between the three stratocumulus regimes, an artefact of the clustering procedure.

Cloud regimes are allocated based on the methodology of Williams and Webb (2009). The joint CTP-τ histograms produced by COSP are averaged according to their bin-centre values to obtain a vector containing gridbox-mean values of CTP, albedo (α), and CF. Albedo values are taken from Williams and Webb (2009), and are derived from the ISCCP simulator code. The gridboxes are then assigned a regime by determining the centroid with the minimum Euclidian distance to this vector.

2.3 Aerosol Forcing by Cloud Regime

2.3.1 Definitions

In this paper we examine the indirect effects of aerosol on clouds, as modelled by the PC2 single moment cloud microphysics scheme within HadGEM3. All functions unless stated otherwise are assumed to be functions of latitude and longitude, and will have these arguments omitted for conciseness.

Following the methods and terminology of Ghan (2013) we define the cloud radiative forcing due to aerosols (ΔC_{clean}) as:

$$\Delta C_{\text{clean}} = \Delta(F_{\text{clean}} - F_{\text{clear,clean}}) \tag{1}$$

where Δ denotes the difference between present-day and pre-industrial emissions periods, C_{clean} denotes the clean-cloud radiative effect, F denotes the net top-of-atmosphere (TOA) radiative flux, and subscripts clean & clear denote the TOA fluxes when the model removes the direct radiative effects of aerosol and cloud respectively.

Relative frequency of occurrence of the k^{th} cloud regime is denoted by $R^k(T)$, and we denote present-day and pre-industrial time periods by T_1 and T_0 respectively. Finally, the cloud radiative effect of the k^{th} regime during time period T, $C^k(T)$ is calculated as:

$$C^k(T) = \frac{\sum_{t \in T} C(t)\delta_{R(t),k}}{\sum_{t \in T} \delta_{R(t),k}} \tag{2}$$

where $R(t)$ is a discrete 10-valued function indicating which cloud regime is seen in each gridbox, δ is the Kronecker delta, and the sum is performed over all timesteps t in the model run representing time period T.

2.3.2 Calculation

It must be possible to recover total clean cloud forcing ERF_{ACI} simply by summing over each regime. ERF_{ACI} is decomposed into a contribution by each regime so that it can be written out as:

$$\Delta C_{\text{clean}} = \sum_k R^k(T_1)C^k(T_1) - R^k(T_0)C^k(T_0) \tag{3}$$

Having done this, it makes sense to define the total forcing by each cloud regime $\Delta C^k_{\text{clean}}$, to be the summand of (3). However, this definition is a little non-physical and it makes more sense to further break down the forcing into individual effects. These proposed effects are:

1. Total forcing resulting from the mean properties within each cloud regime changing, ΔC^k_α.
2. Total forcing resulting from the changing RFO of each cloud regime, ΔC^k_{RFO}.
3. Any additional terms required to recover (3), representing nonlinear interactions.

Therefore, defining $\Delta R^k = R^k(T_1) - R^k(T_0)$, and analogously $\Delta C^k = C^k(T_1) - C^k(T_0)$, this becomes:

$$\Delta C^k_\alpha = R^k(T_0)\Delta C^k \tag{4}$$

$$\Delta C^k_{\text{RFO}} = C^k(T_0)\Delta R^k \tag{5}$$

$$\Delta C^k_{\text{clean}} = \Delta C^k_\alpha + \Delta C^k_{\text{RFO}} + \Delta R^k \Delta C^k \tag{6}$$

$$= R^k(T_0)\Delta C^k + C^k(T_0)\Delta R^k + \Delta R^k \Delta C^k \tag{7}$$

Multiplying out the terms of $\Delta C^k_{\text{clean}}$ and summing over k, one eventually recovers the expression given in (3).

3 Results

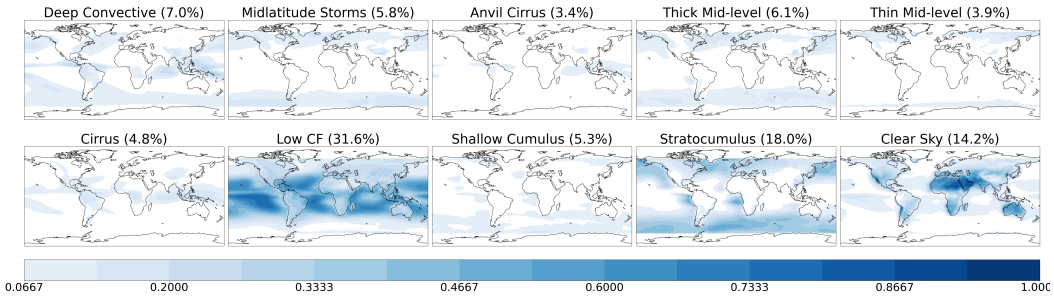

Figure 2. HadGEM-UKCA simulated relative frequency of occurrence of each of the cloud regimes defined in figure 2 in the present-day simulation, including the clear-sky regime, allocated to gridboxes with $CF \leqslant 0.5\%$.

Figure 2 shows the RFO of the 10 regimes used in the analysis in the present-day simulation. This shows that HadGEM3 broadly reproduces the satellite retrieved patterns seen in Tselioudis et al. (2013) throughout the tropics, especially in the cases of deep convection, anvil cirrus clouds, and the low CF regime, which represents regimes with a mixture of shallow cumulus and cirrus clouds. In the mid and high latitudes however, the k-means algorithm struggles to differentiate between deep convection and midlatitude storms. The dominant cloud regimes are the low CF regime, and the stratocumulus regime, primarily seen over the southern ocean and in the marine stratocumulus regions off the west coasts of Africa, North, and South America. There is a small discrepancy in the RFO of thin cloud regimes, however this can be attributed to the different ways with which MODIS and ISCCP detect thin clouds.

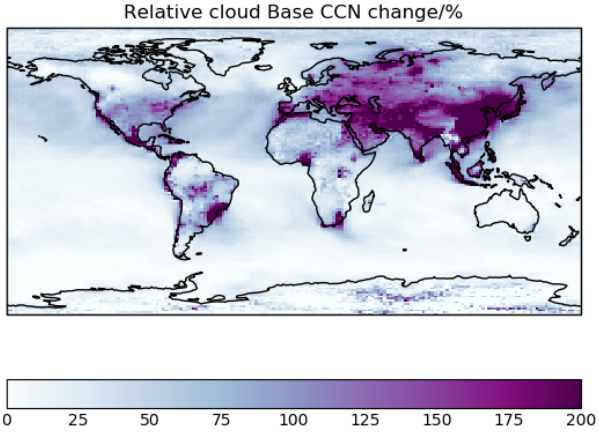

Figure 3. Change in simulated CCN concentration at cloud base in present day relative to pre-industrial aerosol conditions. CCN is defined by the dry particle cutoff radius being larger than 50nm.

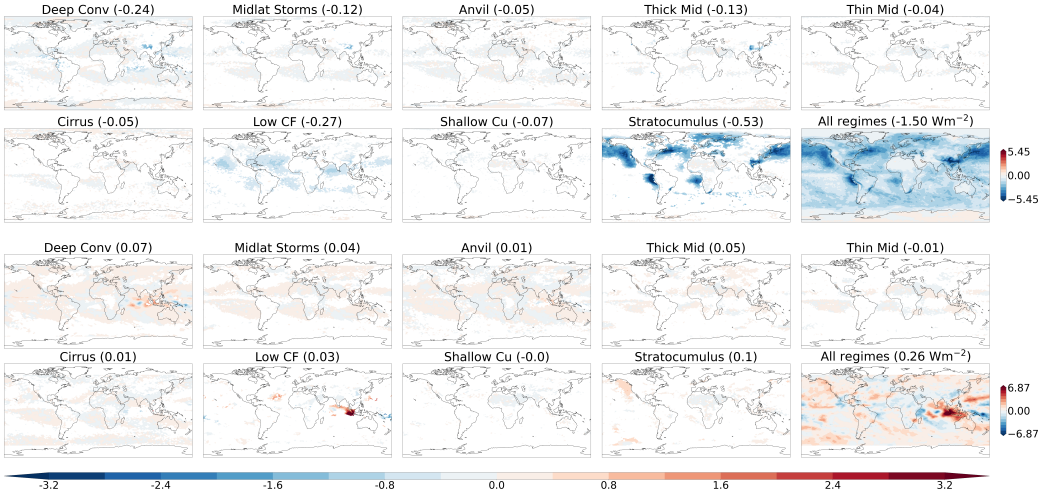

Figure 4. Indirect aerosol forcing arising from changes in regime mean properties for both shortwave (top) and longwave (bottom), ΔC_α^k. The horizontal colourbar shows values for each individual regime, while the vertical colourbar shows values for all regimes combined. The clear regime has been omitted as it produces no forcing.

Figure 3 shows the increase in CCN at cloud base between PD and PI simulations. CCN is defined by the dry particle cutoff radius being larger than 50nm. The strongest increase is seen over land, predominantly over China and south-east Asia, and the Indian subcontinent, with other more localised perturbations seen elsewhere over areas with high emissions. The Southern ocean sees very little aerosol perturbation, and the north Atlantic and Pacific see a perturbation an order of magnitude smaller than the one seen over land.

Figure 4 shows both shortwave and longwave contributions to the forcing produced by changes to mean properties of each cloud regime, as given in (4). The clear-sky regime has been omitted due to the fact that a clear gridbox will produce no $\mathrm{ERF_{ACI}}$. The data is aggregated for each month, and then subjected to a 2-tailed t-test. The data shown is all data which is significant at the 10% level. The forcing is dominated by the shortwave contribution by the stratocumulus regime, particularly in the marine stratocumulus decks off the coast of Africa and North & South America, and in the north Pacific and north Atlantic shipping lanes. The longwave contribution is much smaller than the shortwave, and is more pronounced in regimes with high CF, for instance the stratocumulus or thick mid-level cloud regimes.

The low CF regime contributes about 50% of the forcing of the stratocumulus regime to SW $\mathrm{ERF_{ACI}}$, however has almost no contribution to the LW forcing, except for a distinct signal in the Indo-Pacific warm pool region.

Figure 5 shows the shortwave and longwave contributions to the forcing produced by changes in occurrence of each cloud regime. Once again, this effect is dominated by the shortwave contribution, this time with a roughly equal weighting between the thick mid-level and stratocumulus regimes. Because of the predominantly negative sign of cloud radiative effects, it is easy to see how changes in RFO manifest themselves in forcings. An increased RFO, broadly speaking, will result in an increased negative shortwave forcing, and an increased positive longwave forcing.

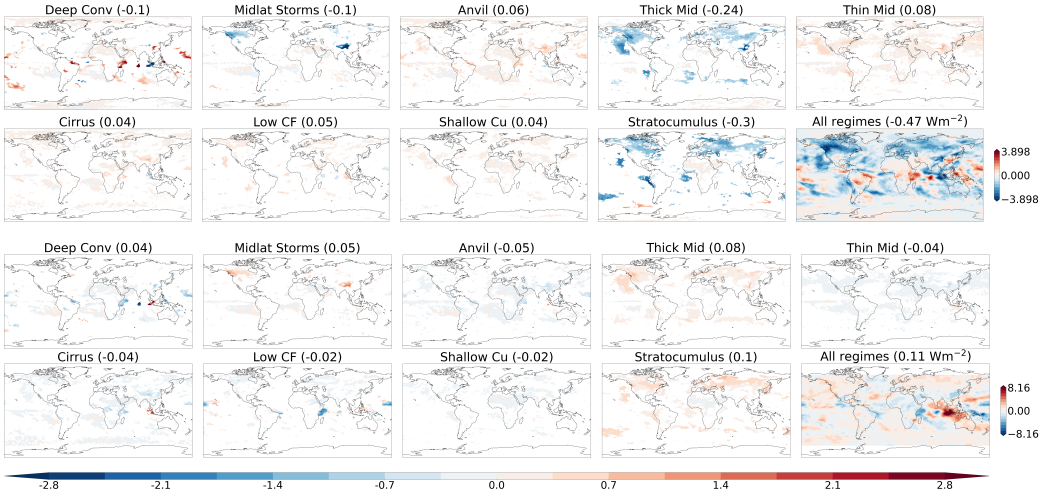

Figure 5. Indirect aerosol forcing arising from changes in RFO of each regime, $\Delta C^k_{\mathrm{RFO}}$. Colourbars are as in figure 4.

This effect is most visible in the mid-level cloud, where the forcing patterns in the thin and thick mid-level cloud regimes map onto each other fairly well. This indicates that for mid-level clouds, HadGEM3 predicts that the increased anthropogenic emissions are not causing a fundamental shift in which types of cloud are predominant over a given area, but merely optical thickening of the pre-existing clouds.

This pattern is also seen between the stratocumulus regime, and the low CF and shallow cumulus regimes. In this case this indicates that if a region with low cloud fraction clouds is given an increased aerosol loading, it will have a tendency to increase cloud fraction in this region. Intuitively, it is likely that this is a result of precipitation suppression and increased cloud lifetimes, however it is impossible to diagnose the exact mechanism behind this shift with the data used in this analysis.

Two regimes neglected in discussion so far have been the deep convective and mid-latitude storm regimes. The reason for this is that the aerosol scheme in HadGEM does not interact directly with the convection scheme, meaning that theoretically there should be no change in the properties of convective clouds between the two simulations. However, there are indirect interactions between the two schemes, and this means that while the forcing produced by these regimes are not attributable to noise, these figures may not be reliable and a specific experiment must be run to accurately diagnose the forcing for the convective regimes. In these simulations, the deep convective regime contributes a total of -0.23 Wm^{-2} to the global indirect aerosol forcing.

The nonlinear effect, $\Delta R^k \Delta C^k$, is $\mathcal{O}(0.01\mathrm{Wm}^{-2})$ and so is not a dominant contribution to the overall forcing.

4 Conclusions

Simulated $\mathrm{ERF}_{\mathrm{ACI}}$ was broken down into contributions from a set of 10 observational cloud regimes. This is further broken down into both shortwave and longwave effects, and into two contributions with physically understandable definitions.

From this analysis it can be concluded that a large majority of forcing in the HadGEM3 GA7.1 comes from changes to the stratocumulus and mid-level cloud regimes (amount-

ing to a total of -0.75 and -0.31 Wm^{-2} respectively). These two sets of regimes have a similar geographical distribution and there may be some crossover between the two regimes, owing to the simplicity of the allocation method.

There is a lesser contribution from the low CF regime, which contributes -0.22 Wm^{-2} to the global ERF_{ACI}. This means that efforts should be focused on constraining the forcing produced specifically by these cloud regimes.

Comparing Figure 3 with the forcing plots, it can be inferred that the sensitivity of ERF_{ACI} to an increased aerosol loading is much greater in marine stratocumulus than in similar clouds seen over land.

Questions remain over whether these findings are universal in modern GCMs, or whether aerosol-cloud interactions manifest themselves differently between different models, and this will be the topic of ongoing research.

Acknowledgments

This work was supported by the Natural Environment Research Council [grant number NE/RO11885/1].

PS and DWP acknowledge funding from NERC projects NE/L01355X/1 (CLARIFY) and NE/P013406/1 (A-CURE). PS additionally acknowledges support from the ERC project RECAP and the FORCeS project under the European Union's Horizon 2020 research programme with grant agreements 724602 and 821205, respectively. JPM was supported by the Met Office Hadley Centre Climate Programme funded by BEIS and Defra (GA01101).

Raw simulation output data from the HadGEM3 model runs are available as Met Office postprocessing data format (.pp; Met Office, 2013) from the JASMIN data infrastructure (http://www.jasmin.ac.uk). The data used to generate the plots used in this paper is publicly available at https://doi.org/10.5281/zenodo.3988192

References

Abdul-Razzak, H., & Ghan, S. J. (2000). A parameterization of aerosol activation: 2. multiple aerosol types. *Journal of Geophysical Research: Atmospheres*, *105*(D5), 6837–6844.

Albrecht, B. A. (1989). Aerosols, cloud microphysics, and fractional cloudiness. *Science*, *245*(4923), 1227–1230. Retrieved from `http://science.sciencemag.org/content/245/4923/1227` doi: 10.1126/science.245.4923.1227

Anderberg, M. R. (2014). *Cluster analysis for applications: probability and mathematical statistics: a series of monographs and textbooks* (Vol. 19). Academic press.

Bellouin, N., Quaas, J., Gryspeerdt, E., Kinne, S., Stier, P., Watson-Parris, D., ... others (2020). Bounding global aerosol radiative forcing of climate change. *Reviews of Geophysics*, *58*(1), e2019RG000660.

Bodas-Salcedo, A., Webb, M., Bony, S., Chepfer, H., Dufresne, J.-L., Klein, S., ... others (2011). Cosp: Satellite simulation software for model assessment. *Bulletin of the American Meteorological Society*, *92*(8), 1023–1043.

Boucher, O., Randall, D., Artaxo, P., Bretherton, C., Feingold, G., Forster, P., ... others (2013). Clouds and aerosols. In *Climate change 2013: the physical science basis. contribution of working group i to the fifth assessment report of the intergovernmental panel on climate change* (pp. 571–657). Cambridge University Press.

Ghan, S. J. (2013). Estimating aerosol effects on cloud radiative forcing. *Atmospheric Chemistry and Physics*, *13*(19), 9971–9974.

Gryspeerdt, E., & Stier, P. (2012). Regime-based analysis of aerosol-cloud interactions. *Geophysical Research Letters*, *39*(21).

Hoesly, R. M., Smith, S. J., Feng, L., Klimont, Z., Janssens-Maenhout, G., Pitkanen, T., ... others (2018). Historical (1750–2014) anthropogenic emissions of reactive gases and aerosols from the community emissions data system (ceds). *Geoscientific Model Development (Online)*, *11*(PNNL-SA-123932).

IPCC. (2013). Summary for policymakers [Book Section]. In T. Stocker et al. (Eds.), *Climate change 2013: The physical science basis. contribution of working group i to the fifth assessment report of the intergovernmental panel on climate change* (p. 130). Cambridge, United Kingdom and New York, NY, USA: Cambridge University Press. Retrieved from `www.climatechange2013.org` doi: 10.1017/CBO9781107415324.004

Jakob, C., & Tselioudis, G. (2003). Objective identification of cloud regimes in the tropical western pacific. *Geophysical Research Letters*, *30*(21).

Mann, G., Carslaw, K., Spracklen, D., Ridley, D., Manktelow, P., Chipperfield, M., ... Johnson, C. (2010). Description and evaluation of glomap-mode: A modal global aerosol microphysics model for the ukca composition-climate model. *Geoscientific Model Development*, *3*(2), 519.

Mulcahy, J., Jones, C., Sellar, A., Johnson, B., Boutle, I., Jones, A., ... others (2018). Improved aerosol processes and effective radiative forcing in hadgem3 and ukesm1. *Journal of Advances in Modeling Earth Systems*, *10*(11), 2786–2805.

Oreopoulos, L., Cho, N., & Lee, D. (2020). A global survey of apparent aerosol-cloud interaction signals. *Journal of Geophysical Research: Atmospheres*, *125*(1), e2019JD031287.

Rossow, W. B., & Schiffer, R. A. (1999). Advances in understanding clouds from isccp. *Bulletin of the American Meteorological Society*, *80*(11), 2261–2288.

Rotstayn, L. D. (1999). Indirect forcing by anthropogenic aerosols: A global climate model calculation of the effective-radius and cloud-lifetime effects. *Journal of Geophysical Research: Atmospheres*, *104*(D8), 9369–9380.

Schuddeboom, A., McDonald, A. J., Morgenstern, O., Harvey, M., & Parsons, S. (2018). Regional regime-based evaluation of present-day general circulation model cloud simulations using self-organizing maps. *Journal of Geophysical Research: Atmospheres*, *123*(8), 4259–4272.

Tselioudis, G., Rossow, W., Zhang, Y., & Konsta, D. (2013). Global weather states and their properties from passive and active satellite cloud retrievals. *Journal of Climate*, *26*(19), 7734–7746.

Twomey, S. (1977). The influence of pollution on the shortwave albedo of clouds. *Journal of the Atmospheric Sciences*, *34*(7), 1149-1152. Retrieved from `https://doi.org/10.1175/1520-0469(1977)034<1149:TIOPOT>2.0.CO;2` doi: 10.1175/1520-0469(1977)034⟨1149:TIOPOT⟩2.0.CO;2

Walters, D., Baran, A. J., Boutle, I., Brooks, M., Earnshaw, P., Edwards, J., ... others (2019). The met office unified model global atmosphere 7.0/7.1 and jules global land 7.0 configurations. *Geoscientific Model Development*, *12*(5), 1909–1963.

West, R., Stier, P., Jones, A., Johnson, C., Mann, G., & Bellouin, N. (2014). Dg 992 partridge, and z. kipling (2014), the importance of vertical velocity variability 993 for estimates of the indirect aerosol effects. *Atmospheric Chemistry and Physics*, *994*.

Williams, K. D., & Webb, M. J. (2009, Jul 01). A quantitative performance assessment of cloud regimes in climate models. *Climate Dynamics*, *33*(1), 141–157. Retrieved from `https://doi.org/10.1007/s00382-008-0443-1` doi: 10.1007/s00382-008-0443-1

Wilson, D. R., Bushell, A. C., Kerr-Munslow, A. M., Price, J. D., & Morcrette, C. J. (2008). Pc2: A prognostic cloud fraction and condensation scheme. i: Scheme

description. *Quarterly Journal of the Royal Meteorological Society: A journal of the atmospheric sciences, applied meteorology and physical oceanography*, *134*(637), 2093–2107.